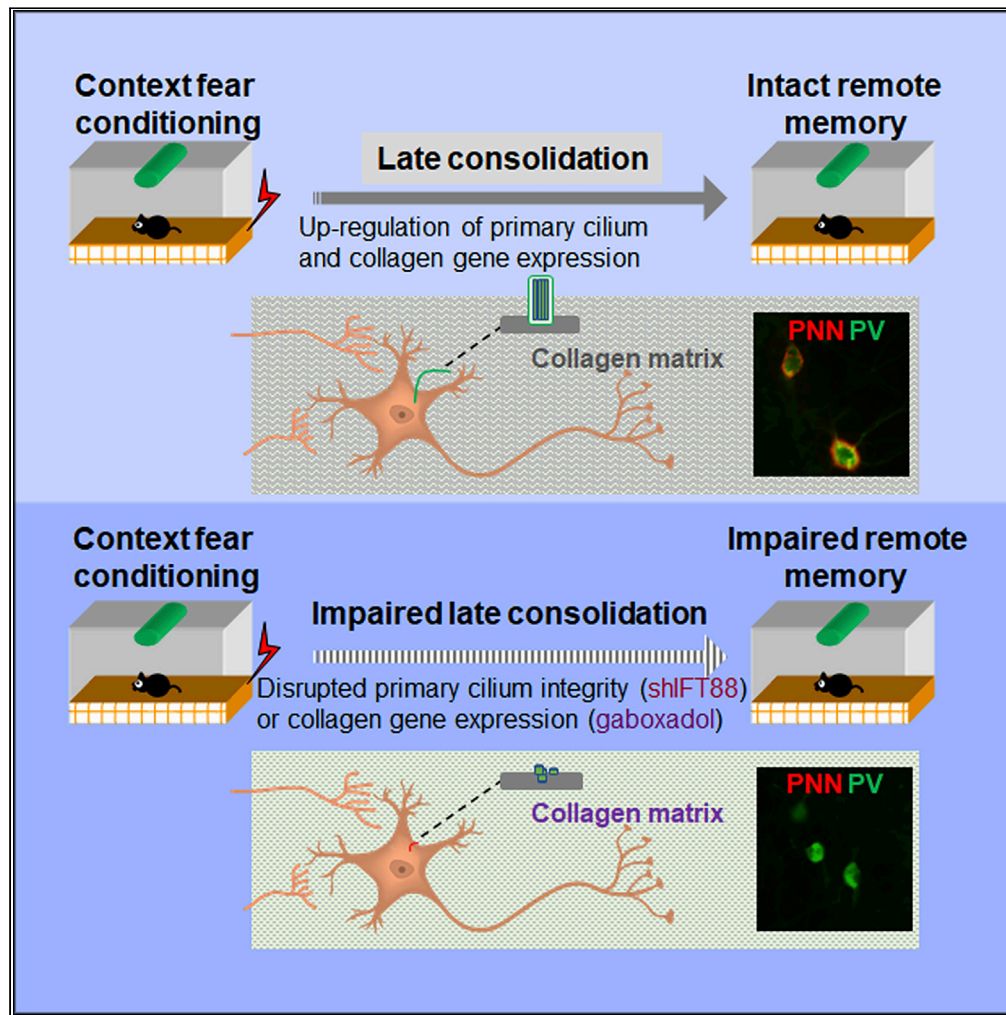


Article

Primary cilia are required for the persistence of memory and stabilization of perineuronal nets



Vladimir Jovasevic, Hui Zhang, Farahnaz Sananbenesi, ..., John E. Wiktorowicz, Andre Fischer, Jelena Radulovic

jovasevicv@gmail.com (V.J.)
jelena.radulovic@einsteinmed.org (J.R.)

Highlights

Changes in the cytoskeleton progressively expand during memory consolidation

Primary cilium-associated genes are upregulated in remote vs recent memory

The primary cilium supports the role of the hippocampus in long-term consolidation

The primary cilium has a critical role in the organization and/or stability of PNNs

Jovasevic et al., iScience 24, 102617
June 25, 2021 © 2021 The Authors.
<https://doi.org/10.1016/j.isci.2021.102617>

Article

Primary cilia are required for the persistence of memory and stabilization of perineuronal nets

Vladimir Jovasevic,^{1,*} Hui Zhang,² Farahnaz Sananbenesi,³ Anita L. Guedea,⁴ Kizhake V. Soman,⁵ John E. Wiktorowicz,⁶ Andre Fischer,³ and Jelena Radulovic^{1,2,7,*}

SUMMARY

It is well established that the formation of episodic memories requires multiple hippocampal mechanisms operating on different time scales. Early mechanisms of memory formation (synaptic consolidation) have been extensively characterized. However, delayed mechanisms, which maintain hippocampal activity as memories stabilize in cortical circuits, are not well understood. Here we demonstrate that contrary to the transient expression of early- and delayed-response genes, the expression of cytoskeleton- and extracellular matrix-associated genes remains dynamic even at remote time points. The most profound expression changes clustered around primary cilium-associated and collagen genes. These genes most likely contribute to memory by stabilizing perineuronal nets in the dorsohippocampal CA1 subfield, as revealed by targeted disruptions of the primary cilium or perineuronal nets. The findings show that nonsynaptic, primary cilium-mediated mechanisms are required for the persistence of context memory.

INTRODUCTION

Over time, representations of personal experiences are either forgotten or transition from labile to persistent episodic memories. This process initially involves synaptic molecular changes in the hippocampus (synaptic consolidation), which are followed by the hippocampally-guided reorganization of cortical circuits that support memories (systems consolidation) (Frankland and Bontempi, 2005; Remondes and Schuman, 2004). However, the mechanisms of memory consolidation as memories transition from recent to remote are not well understood. This is particularly important in the case of negatively and positively valenced memories, which have a profound impact on affect and motivated behavior.

Many animal models have been developed to induce long-lasting memories of stressful experiences in order to understand their underlying molecular mechanisms (Poulos et al., 2016; Radulovic and Tronson, 2010; Revest et al., 2010; Sullivan et al., 2017), especially models of hippocampus-dependent memory, such as contextual fear conditioning (FC) (Frankland and Bontempi, 2005; Tonegawa et al., 2018). Multiple transcriptome analyses in the hippocampus following fear conditioning have been performed to date with the purpose of defining the mechanisms of synaptic consolidation (Barnes et al., 2012; Cho et al., 2015; Federighi et al., 2013; Levenson et al., 2004; Mei et al., 2005; Peixoto et al., 2015; Poplawski et al., 2016; Rao-Ruiz et al., 2019). However, the latest time point for transcriptome analyses thus far was seven days after fear conditioning (Mizuno et al., 2020); therefore, gene expression patterns that accompany the later stages of memory processing as they transition from recent to remote have remained largely unknown, although changes in gene expression seem likely given that the consolidation of remote memories entails genome-wide histone modifications (Halder et al., 2016b).

Alterations of the cytoskeleton have been extensively demonstrated in processes related to synaptic consolidation (Bi et al., 2010; Fanara et al., 2010; Fischer et al., 2004; Hou et al., 2009; Nelson et al., 2012; Shumyatsky et al., 2005; Uchida et al., 2014). Hippocampal glutamate receptor activity and cAMP-dependent protein kinase (PKA) signaling (Abel et al., 1997; Impey et al., 1998) trigger synaptic strengthening in the hours after acquisition. These activity-dependent changes in spine morphology require the rearrangement of actin filaments (AFs) (Matus, 2000; Tada and Sheng, 2006), which are regulated by dynamic microtubules (MTs) and end-binding protein 3 (EB3) (Jaworski et al., 2009). Involvement of the cytoskeleton and its changes in remote memory has been studied to a lesser extent. Nevertheless, existing data suggest that alterations of the cytoskeleton contribute to these processes as well. For example, the loss of

¹Department of Pharmacology, Feinberg School of Medicine, Northwestern University, Room 13-100, Montgomery Ward Memorial Building, Chicago, IL 60611, USA

²Department of Neuroscience and Department of Psychiatry and Behavioral Sciences, Albert Einstein College of Medicine, Rose F. Kennedy Center, 1410 Pelham Parkway South, Room 115, Bronx, NY 10461, USA

³German Center for Neurodegenerative Diseases, Göttingen 37075, Germany

⁴Department of Psychiatry and Behavioral Sciences, Northwestern University, Chicago, IL 60611, USA

⁵Division of Infectious Disease, Department of Internal Medicine, UTMB – Galveston, Galveston, TX 77555, USA

⁶InnovaRegi, LLC, San Jose, CA 95138, USA

⁷Lead contact

*Correspondence: jovasevicv@gmail.com (V.J.), jelena.radulovic@einsteinmed.org (J.R.)
<https://doi.org/10.1016/j.isci.2021.102617>



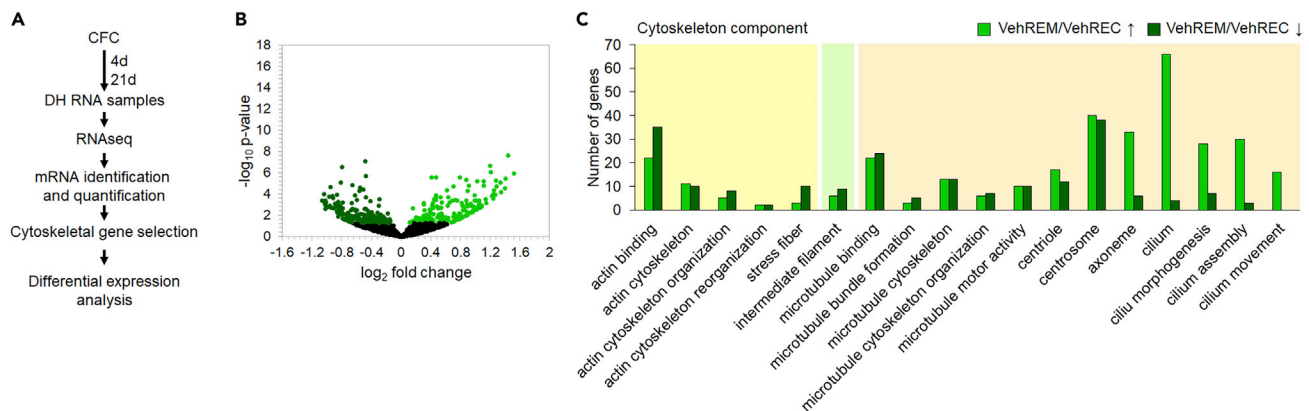


Figure 1. RNAseq analysis of the expression of cytoskeleton-associated genes

(A) Experimental outline for gene expression analysis.

(B) Gene expression differences between remote and recent memory are shown in a volcano plot. Genes whose expression was altered significantly ($p < 0.05$) are indicated in green.

(C) Cytoskeletal component GO term analysis of differentially expressed genes in remote vs recent memory. GO terms were grouped based on their association with AF (yellow), IF (green), or MT (purple).

See also [Table S1](#).

cdc42 has been shown to specifically impair remote memory, suggesting active actin remodeling at this time point (Kim et al., 2014). Also, inhibition of miR-598-3p blocks the retrieval of remote fear memory. This miRNA targets numerous genes involved in actin remodeling, again suggesting a dynamic cytoskeleton and its functional relevance in remote memory (Jones et al., 2019). Together, these studies suggest that ongoing cytoskeletal dynamics might contribute to the stabilization of memories as they transition from recent to remote.

We tested this possibility by investigating the transcriptional dynamics of hippocampal cytoskeleton-associated genes during memory consolidation. High throughput analyses of the changes in cytoskeleton-associated gene expression in the dorsal hippocampus (DH) demonstrated that MT-associated genes undergo the most substantial changes, particularly those associated with the integrity and function of the primary cilium. By specifically depleting primary cilia in the hippocampal CA1 subfield, we demonstrated that this organelle plays an important role in delayed, but not early, hippocampal activity required for the persistence of memory. This effect was accompanied by disruption of perineuronal nets (PNN) in CA1 but not in other hippocampal subfields. Lastly, we demonstrate that failure to form lasting memories is accompanied by profound downregulation of primary cilium-associated genes as well as genes coding for several collagens, important constituents of PNN.

RESULTS

Differential expression of cytoskeleton-associated genes during memory consolidation from recent to remote

We analyzed the expression of cytoskeleton-associated genes four (recent) or twenty-one days (remote memory) after training (Figure 1A). Detected RNAs were matched against MGI database to select genes associated with the cytoskeleton, identifying 1,590 genes (Table S1). Among these genes, 342 genes showed significant changes in the expression level between remote and recent memory (Figure 1B).

In order to identify cytoskeletal systems involved in the transition of memory from recent to remote, we analyzed the genes whose expression was altered in remote, relative to recent, memory for their association with cytoskeletal components. Differentially expressed genes were associated with AFs and MTs, and to a much lesser extent with intermediate filaments. The most striking observation was that the strongest association of these differentially expressed genes was with primary cilium-associated processes, and most of these genes were upregulated in remote memory (Figure 1C and Table S2), suggesting different roles of the primary cilium at these two stages. We therefore went on to determine whether this is the case. We depleted the primary cilium specifically from the CA1 region of DH, since CA1 is critically involved in

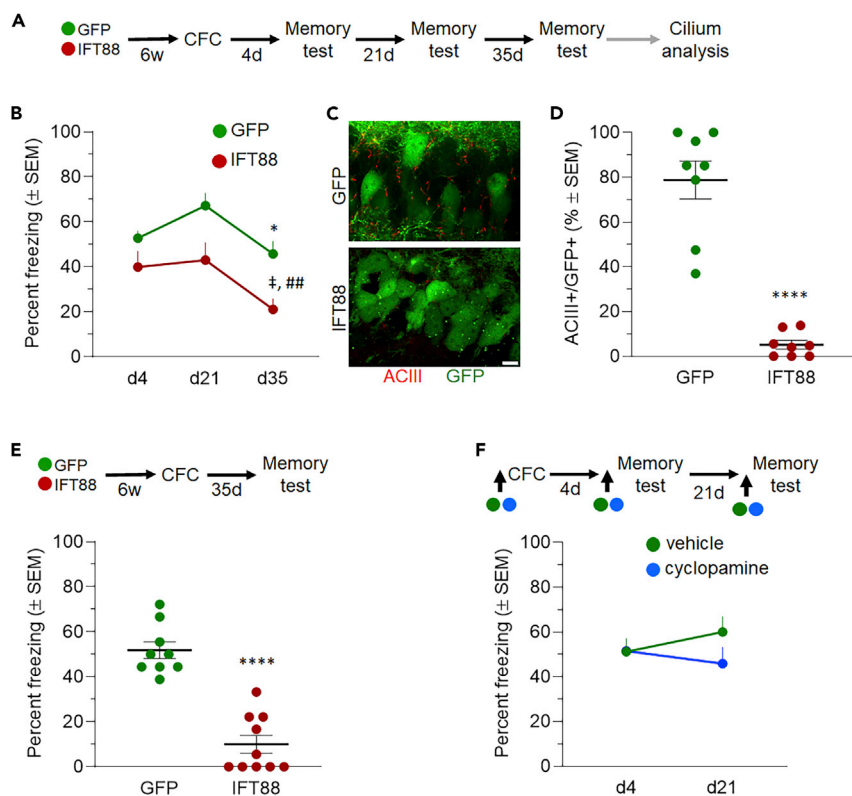


Figure 2. The role of the primary cilium in recent and remote memory

(A) Experimental outline: AAV vector expressing control (GFP) or shIFT88 (IFT88) RNA was infused into CA1. Six weeks later mice were fear conditioned, and tested 4, 21 and 35 days later.

(B) Effect of the primary cilium depletion from CA1 on memory. Mice infused into CA1 with control or shIFT88 AAV were fear conditioned, and tested at recent and remote time points. Data are represented as mean \pm SEM (repeated measures two-way ANOVA, $n = 10$ /group, effect of virus: $F_{2, 36} = 1.351$, $p = 0.0070$; effect of day: $F_{1, 917, 34, 51} = 14.13$, $P < 0.0001$; post-hoc: $*p = 0.0110$ D35 GFP vs IFT88, $^{\ddagger}p = 0.0251$ IFT88 D35 vs D4, $^{##}p = 0.0025$ IFT88 D21 vs D35).

(C) Representative images demonstrating the depletion of primary cilia from CA1 region of DH. Size bar: $5 \mu\text{m}$.

(D) Quantification of the shIFT88 RNA effect. Data are represented as mean \pm SEM. $****P < 0.0001$ (unpaired ttest, two-tailed; $n = 8$ /group; $t_{14} = 8.466$).

(E) Effect of the primary cilium depletion from CA1 on remote memory. Mice infused into CA1 with control or shIFT88 AAV were fear conditioned, and tested at remote time point only. Data are represented as mean \pm SEM (unpaired ttest, two-tailed; $n = 9$ (GFP), $n = 10$ (IFT88)/group; $t_{17} = 7.674$; $****P < 0.0001$).

(F) Effect of cycloamine infusion into CA1 on recent and remote memory retrieval. Data are represented as mean \pm SEM (two-way ANOVA, $n = 9$ /group, effect of treatment $F_{1, 14} = 3.182$ $p = 0.0962$; effect of day $F_{1, 14} = 1.755$, $p = 0.2065$).

See also [Figures S1–S3A](#) and [S3B](#).

retrieval and consolidation of contextual memories, whereas CA3 seems to be important at the earliest stage of acquisition, with a smaller role in retrieval of contextual memories past 24 h time point (Daumas et al., 2005; Ji and Maren, 2008; Lee and Kesner, 2004). For this purpose, we used an AAV vector expressing shRNA targeting intraflagellar transport 88 (IFT88) gene, which is essential for the formation and function of primary cilium (Haycraft et al., 2007) (Figure S1). AAV vectors did not exhibit cell toxicity, as revealed by viable and healthy primary hippocampal neurons transduced with control (GFP) or shIFT88 (IFT88) vectors (Figure S2). The AAV infusion resulted in a substantial reduction in the number of primary cilia (Figures 2C and 2D). Mice were trained in contextual fear conditioning paradigm and tested at recent and remote time points (Figure 2A). Primary cilium depletion did not affect locomotor activity or response to electric shock (Figures S3A and S3B). Freezing in shIFT88 group was not significantly different from the control at recent memory test, indicating that the primary cilium is dispensable for encoding and in recent memory (Figure 2B). In contrast, depletion of primary cilia impaired remote memory, and this impairment increased gradually from day 21 to day 35. Because we tested mice repeatedly at three time points, the decreased freezing in shIFT88 group at remote time may result from impaired reconsolidation and/or facilitated

extinction. To exclude this possibility, we trained mice following control or shIFT88 AAV infusion, and tested only at the remote time point. As in the previous experiment, primary cilium depletion did not affect locomotor activity or response to electric shock (Figures S3C and S3D). We observed a strong memory impairment (Figure 2E), indicating that the primary cilium depletion specifically affects remote memory.

Since shIFT88-mediated depletion of the primary cilium takes place before the initiation of the behavioral experiments, the observed memory impairment could be attributed to the deficits in memory consolidation or retrieval. To evaluate the role of the primary cilium in retrieval, we blocked sonic hedgehog (Shh) signaling specifically prior to memory tests. Shh is the signaling pathway most strongly linked to the primary cilium (Louvi and Grove, 2011), and which regulates neuronal functions in the adult brain (Breunig et al., 2008; Petrova and Joyner, 2014), including neuronal firing rate (Bezard et al., 2003), and hippocampal neuroplasticity (Yao et al., 2016). Inhibition of Shh prior to either recent or remote memory test did not impair memory (Figure 2F), suggesting that the primary cilium does not mediate memory retrieval. Together, these results suggest that the MT network contributes to the persistence of memory through non-synaptic mechanisms, with primary cilium playing a central role.

Primary cilium regulation of extracellular matrix

The primary cilium has access to a different extracellular environment relative to synaptic structures, especially to various components of the extracellular matrix (ECM), which undergoes extensive reorganization during memory consolidation (Nguyen et al., 2020; Tsien, 2013), and regulates synaptic plasticity (Dityatev and Rusakov, 2011). The primary cilium is an important mediator of ECM composition and dynamics, either by mediating ECM protein trafficking and secretion (Noda et al., 2016; Smits et al., 2010), or through the transcriptional control of the expression of ECM-degrading proteases (Chang et al., 2012; Rockel et al., 2016), suggesting that the primary cilium may be involved in memory consolidation through the regulation of ECM. Our RNAseq analysis identified 93 differentially expressed ECM-associated genes in remote vs. recent memory (Figure 3A and Table S3). Pathway network analysis of differentially expressed genes associated with the primary cilium or ECM demonstrate an extensive interconnection between the two clusters (Figure 3B), suggesting a strong cross-communication. The ECM-associated genes were clustered in pathways regulating ECM restructuring, including organization and degradation of ECM, as well as ECM proteoglycans (Table 1).

Brain ECM is a highly organized system that consists of collagens, noncollagenous proteins, glycoproteins, hyaluronan, and proteoglycans (Novak and Kaye, 2000; Sethi and Zaia, 2017). Chondroitin sulfate proteoglycans (CSPGs) are a major class of ECM proteins in the brain (Kelwick et al., 2015; Levy et al., 2014), and are expressed prominently in perineuronal nets (PNNs) (Reichelt et al., 2019). Although not the most abundant constituent of PNNs, collagens are essential for their proper organization (Murakami et al., 1999; Su et al., 2017). PNNs have an important role in memory processing (Hylin et al., 2013; Romberg et al., 2013; Thompson et al., 2018), and are postulated to be molecular substrates for long-term memory storage (Tsien, 2013). Therefore, we tested whether the disruption of the primary cilium in the CA1 region affects the organization of PNNs. IFT88 knockdown resulted in a very substantial reduction in the number of PNNs in CA1 (Figures 3C and 3D, S4). At the same time, the organization of PNNs in the dentate gyrus (DG) where the AAV constructs were not expressed was not different between the groups. These results suggest that the primary cilium mediates memory consolidation through the regulation of PNN dynamics in the CA1 region of DH. To determine the role of CA1 PNNs in recent and remote memory, we infused chondroitinase ABC, trained and tested mice at the recent or remote time point, using separate sets of mice for each of the four experimental groups. Chondroitinase ABC treatment resulted in a strong depletion of PNNs from CA1 (Figure 3F). We observed substantial impairment of remote, but not of recent memory (Figure 3E), indicating selective involvement of PNNs in remote memory. Distribution of PNNs in the hippocampus of the N-methyl D-aspartate glutamate receptor, subunit 2A (NR2A) knockdown mouse was not different from those of control mice (Figure S5), providing additional support for the synaptic transmission-independent mechanism through which the primary cilium, and consequently PNNs, regulate memory consolidation. It is noteworthy that the largest cluster of genes up-regulated during remote memory contained numerous collagens, or collagen-regulating genes (Table 1 and Figures S6A and S6B), suggesting that the stabilization of memories and PNN is more likely to be mediated by collagen rather than CSPGs constituent of PNNs.

Effect of impaired consolidation on primary cilium gene expression and function

The next set of experiments was performed to determine the pattern of cytoskeletal gene expression in a model of state-dependent memory characterized by impaired systems consolidation. Such memories are typically acquired during increased tonic inhibition in the hippocampus induced by gaboxadol, an agonist

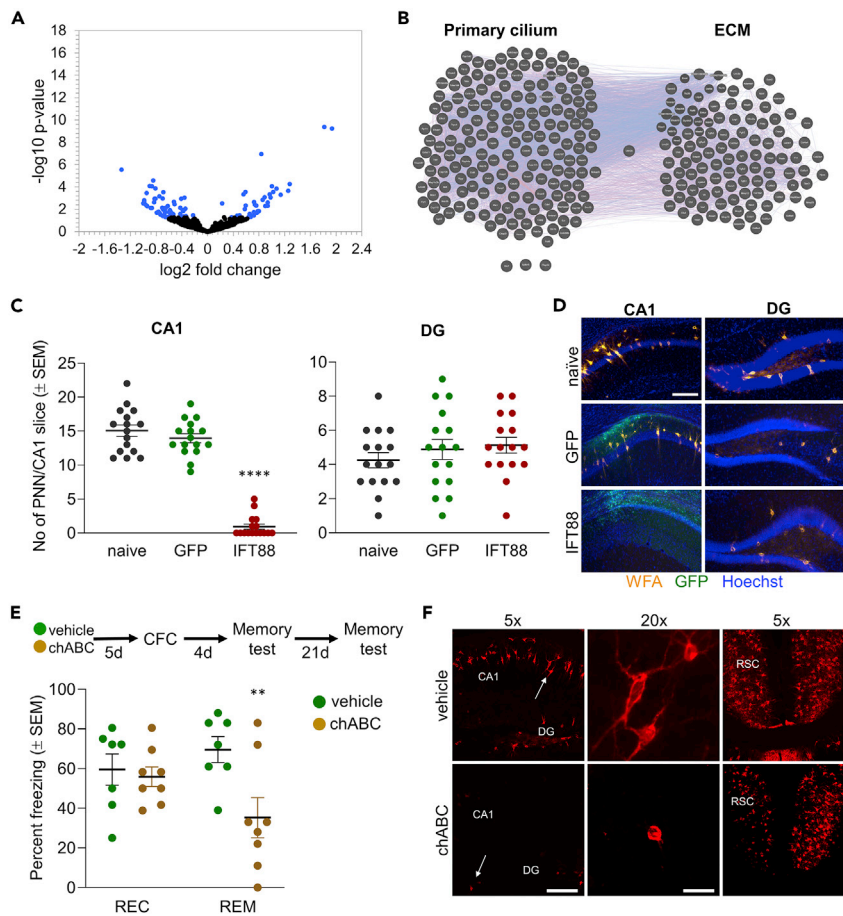


Figure 3. Regulation of ECM by the primary cilium

(A) Gene expression differences between remote and recent memory are shown in a volcano plot. Genes whose expression was altered significantly ($p < 0.05$) are indicated in blue.

(B) GeneMANIA functional interaction network analysis between genes in “Primary cilium” and “ECM” GO terms. Lines indicate network connections based on co-expression (purple), co-localization (blue), shared protein domains (taupe) and physical interactions (pink).

(C) Quantification of the effect of shIFT88 RNA infused in CA1 on PNNs in CA1 and DG. Data are represented as mean \pm SEM (one-way ANOVA, $n = 16/\text{group}$; CA1: $F_{2, 45} = 147.5$, $p = 0.0153$; DG: $F_{2, 45} = 0.8014$, $p = 0.4550$; **** $P < 0.0001$ vs naive or GFP).

(D) Representative images illustrating the effect of the primary cilium depletion from CA1 region of DH on PNNs in CA1 and DG, comparing untransduced (naive) and AAV-transduced mice. Size bar: 200 μm .

(E) Effect of PNN depletion on recent and remote memory. Mice infused into CA1 with vehicle (ACSF), or chondroitinase ABC were fear conditioned, and tested at recent or remote time point. Separate sets of mice were used for each experimental group. Data are represented as mean \pm SEM (two-way ANOVA, $n = 7$ (vehREC, vehREM), 8 (chABC REC, chABC REM)/group, effect of treatment: $F_{1, 13} = 5.062$, $p = 0.0424$; test \times treatment interaction: $F_{1, 13} = 5.019$, $p = 0.0432$; post-hoc: $p = 0.9332$ chABC REC vs vehREC, ** $p = 0.0080$ chABC REM vs vehREM).

(F) Representative images of PNNs in CA1 and RSC from mice infused into CA1 with vehicle or chondroitinase ABC. Arrows indicate examples of PNNs. Size bar: 150 μm (5 \times), 25 μm (20 \times).

See also [Figures S4–S6A](#) and [S6B](#) and [Table S3](#).

of extrasynaptic GABA_A receptors (Jovasevic et al., 2015; Meyer et al., 2017). In contrast to normal conditions, memories acquired under the influence of gaboxadol remain hippocampus-dependent even at remote time points (Meyer et al., 2017), and their retrieval is suppressed, rather than enhanced, by cortical activity (Jovasevic et al., 2015), suggesting a strong inhibition of systems consolidation.

We first tested how gaboxadol affects the expression of cytoskeleton-associated genes in the DH in remote memory (Figure 4A) and identified 101 genes that were differentially expressed between vehicle- and

Table 1. Significantly over-represented ECM pathways associated with EC genes up- and down-regulated in remote relative to recent memory

Pathway name	Entities			
	Found	Ratio	P	FDR
Collagen chain trimerization	12/41	0.0036616	7.83×10^{-8}	2.46×10^{-5}
NCAM1 interactions	23/09	0.0020541	2.10×10^{-7}	3.30×10^{-5}
Extracellular matrix organization	33/327	0.0292042	8.35×10^{-7}	8.68×10^{-5}
Collagen formation	17/112	0.0100026	1.51×10^{-6}	1.18×10^{-4}
Collagen degradation	12/63	0.0056265	4.05×10^{-6}	2.51×10^{-4}
Collagen biosynthesis and modifying enzymes	13/73	0.0065196	5.11×10^{-6}	2.66×10^{-4}
Assembly of collagen fibrils and other multimeric structures	13/77	0.0068768	6.72×10^{-6}	2.96×10^{-4}
Integrin cell surface interactions	13/82	0.0073233	7.64×10^{-5}	0.002737212
Laminin interactions	28/07	0.0025006	8.05×10^{-5}	0.002737212
Non-integrin membrane-ECM interactions	08/40	0.0035723	1.38×10^{-4}	0.004293298
Degradation of the extracellular matrix	16/154	0.0137536	3.31×10^{-4}	0.009265766
ECM proteoglycans	09/54	0.0048227	3.72×10^{-4}	0.009674899
Platelet degranulation	13/131	0.0116995	0.001057	0.025382976

gaboxadol-conditioned mice (Table S1). GO analysis revealed that among these differentially expressed genes, the strongest association was with the primary cilium related terms, and the majority of these primary cilium-associated genes were downregulated in gaboxadol-conditioned mice (Figure 4B, Table S2). We confirmed these findings by qPCR on four randomly selected primary cilium-associated genes (Figure 4C). Additionally, these results show that in naive mice there was no difference in the expression of these genes, indicating that gaboxadol does not produce a general downregulation of primary cilium genes, but rather results in a specific inhibition of their upregulation in remote memory. We also show that gaboxadol affected the expression of ECM-associated genes in remote memory (Figures S6C and S6D and Table S3). Although fewer genes were differentially regulated in gaboxadol conditioned mice, compared to the genes associated with the primary cilium, most of them were downregulated (31 out of 35 total).

Our analyses suggested that a single injection of gaboxadol at training results in a significant and delayed downregulation of primary cilium function. To better understand the possible causes of such downregulation we also examined the acute and early effects of gaboxadol. We first evaluated its effect on the size of the primary cilium, as an indication of changes in its function (Malicki and Johnson, 2017; Uddin et al., 2019), in unstimulated hippocampal neurons or following stimulation of glutamatergic receptors (Figure 4D). While stimulation of hippocampal neurons resulted in a substantial increase in the size of primary cilium at both 24 h and 48 h time points, gaboxadol treatment completely blocked this increase at 24 h and 48 h (Figures 4E and 4F) without affecting the cilium properties of unstimulated neurons. These results demonstrate an acute inhibitory effect of gaboxadol on the primary cilium, which is likely to precede the downregulation of the primary cilium-associated genes.

To better understand the mechanisms leading to downregulation of cilium-associated genes at remote time points, we also examined the effects of gaboxadol on cytoskeletal dynamics during recent memory by analyzing the abundance and post-translational modifications (phosphorylation and S-nitrosylation [SNO]) of cytoskeletal proteins (Figure 4G). We analyzed phosphorylation level as a major molecular mechanism through which protein function is regulated in response to extracellular stimuli (Schlessinger, 2000), and the most prominent mechanism of neural plasticity (Nestler and Greengard, 1999), and SNO as an antagonistic modification to phosphorylation (Choi et al., 2011; Coultrap and Bayer, 2014; Yasukawa et al., 2005). We identified 12 differentially expressed/modified cytoskeleton-associated proteins (Figure 4H and Table S4). These proteins were primarily associated with actin filaments (Figure 4I). Only one protein, nucleotide binding protein 2 (Nubp2), was associated with cilium GO terms, and its increase in abundance and phosphorylation would suggest increased disruption of cilium function (Kypril et al.,

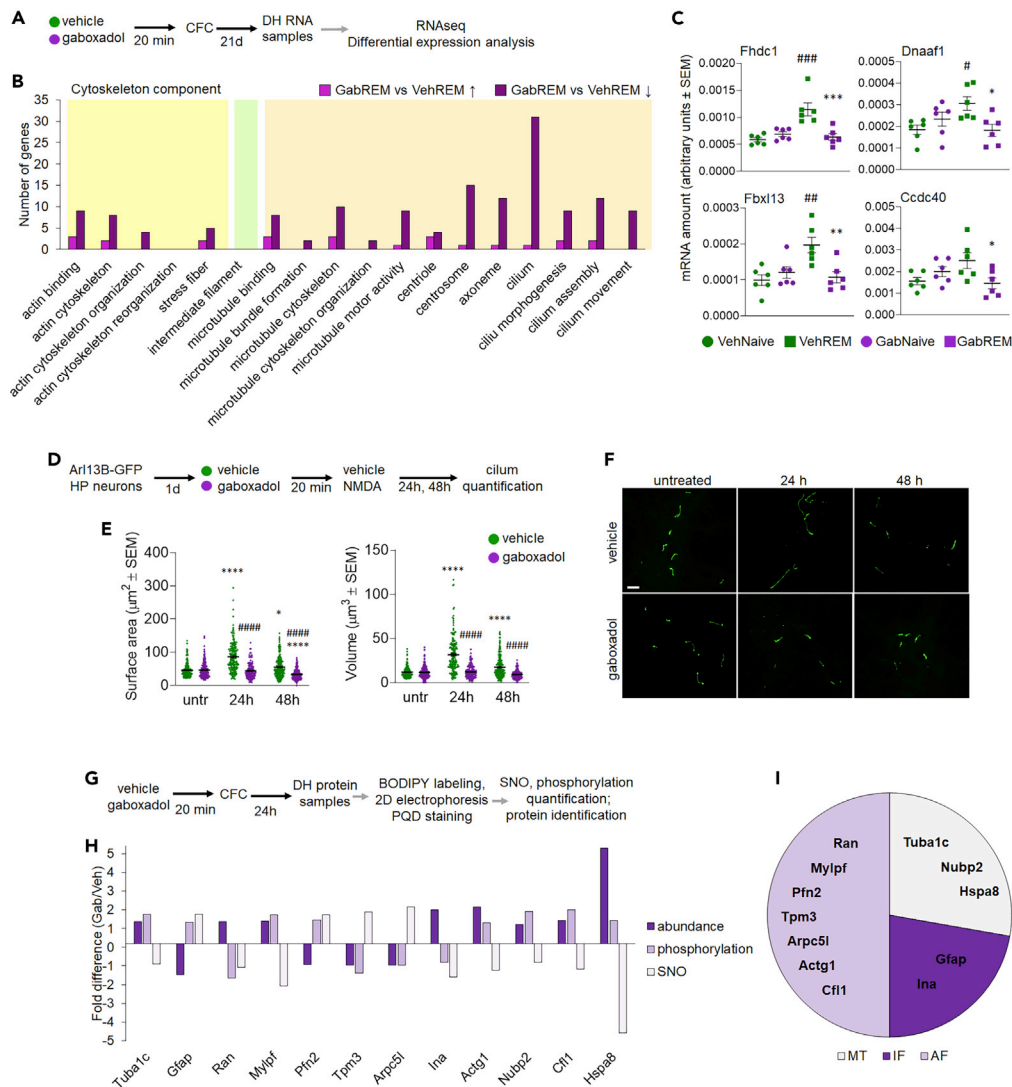


Figure 4. Effect of gaboxadol on primary cilium gene expression and function

(A) Experimental outline.

(B) Cytoskeletal Component GO term analysis of differentially expressed genes at remote memory in vehicle vs gaboxadol. GO terms were grouped based on their association with AF (yellow), IF (green), or MT (purple).

(C) qPCR validation of RNAseq results. Separate set of samples was analyzed for the expression of four randomly selected primary cilium-associated genes. The expression levels in vehicle and gaboxadol groups were compared at remote memory, and in naive mice. Data are represented as mean \pm SEM (one-way ANOVA, $n = 6/\text{group}$; Fhdc1: $F_{3,20} = 12.56$, $P < 0.0001$; Dnaaf1: $F_{3,20} = 4.144$, $p = 0.0195$; Fbx13: $F_{3,20} = 6.817$, $p = 0.0024$; Ccdc40: $F_{3,20} = 3.360$, $p = 0.0392$; post-hoc, Fhdc1: $###p = 0.0001$ vs VehNaive, $***p = 0.0004$ vs VehREM; Dnaaf1: $\#p = 0.0325$ vs VehNaive, $*p = 0.0279$ vs VehREM; Fbx13: post-hoc, Fhdc1: $###p = 0.0034$ vs VehNaive, $**p = 0.0073$ vs VehREM; Ccdc40: $*p = 0.0458$ vs VehREM).

(D–F) Effect of gaboxadol on primary cilium size. (D) Experimental outline: hippocampal neurons from P1 Arl13B-GFP pups were cultured for 14 days, treated with gaboxadol or vehicle 20 min prior to addition of NMDA, stimulated with NMDA for 5 min, and the primary cilium surface area and volume determined 24 or 48 h later. (E) Quantification of the primary cilium size measurements. Data are represented as mean \pm SEM (two-way ANOVA $n = 180/\text{untreated vehicle}$, $n = 216/\text{untreated gaboxadol}$, $n = 168/\text{NMDA 24 h vehicle}$, $n = 131/\text{NMDA 24 h gaboxadol}$, $n = 210/\text{NMDA 48 h vehicle}$, $n = 195/\text{NMDA 48 h gaboxadol}$; NMDA treatment: surface area: $F_{2,1094} = 57.95$, $P < 0.0001$; volume: $F_{2,1094} = 86.51$, $P < 0.0001$; 1 gaboxadol treatment: surface area: $F_{2,1094} = 162.5$, $P < 0.0001$; volume: $F_{2,1094} = 205.5$, $P < 0.0001$; interaction between NMDA and gaboxadol treatments: surface area: $F_{2,1094} = 51.67$, $P < 0.0001$; volume: $F_{2,1094} = 65.34$, $P < 0.0001$; post-hoc: $*P < 0.05$, $***P < 0.0001$ vs untreated; $####P < 0.0001$ vs vehicle of the same time point). (F) Maximum intensity profile of representative Z-stacks. Size bar: 10 μm .

Figure 4. Continued

(G–I) Proteomic analysis identifying differentially expressed, phosphorylated or S-nitrosylated proteins between vehicle and gaboxadol conditioned mice. (G) Experimental outline. (H) Bar graph representation of fold difference in abundance, phosphorylation, or SNO between gaboxadol and vehicle groups. (I) Association of identified cytoskeletal proteins with microtubules (MT), actin filaments (AF), or intermediate filaments (IF).

See also [Figures S6C](#) and [S6D](#), [Table S1](#) and [S2–S4](#).

2014). Collectively, these findings suggest that the early effects of gaboxadol involve early disruption of cilium function and AF dynamics, which precede the delayed downregulation of cilium-associated genes.

DISCUSSION

We provide here comprehensive evidence for dynamic regulation of cytoskeleton-associated genes during the consolidation of fear-provoking memories from recent to remote. We make four key observations: (1) Changes in the cytoskeleton, initiated in early, post-encoding phases, continue and progressively expand over a prolonged period of time, encompassing not only synaptic ([Basu and Lamprecht, 2018](#); [Matus, 2000](#); [Tada and Sheng, 2006](#)) but also nonsynaptic activity; (2) these changes involve a shift from AF-related to MT-related genes, especially those involved in the regulation of the integrity and function of the primary cilium; (3) the primary cilium supports the hippocampal role beyond synaptic consolidation; (4) the primary cilium has a critical role in the organization and/or stability of PNNs.

Transcriptome analyses conducted thus far demonstrate a dynamic but transient process of gene expression early after encoding, with two waves of gene upregulation, which subside by the 24 h time point ([Barnes et al., 2012](#); [Cho et al., 2015](#); [Federighi et al., 2013](#); [Levenson et al., 2004](#); [Mei et al., 2005](#); [Peixoto et al., 2015](#); [Poplawski et al., 2016](#); [Rao-Ruiz et al., 2019](#)). We demonstrate here that cytoskeleton-associated gene expression remains dynamic from the 24 h time point onward. The current model of the role of the cytoskeleton in memory consolidation proposed by [Basu and Lamprecht](#) is that it regulates the formation of new spines following encoding, and is subsequently involved in maintaining spine morphology and memory ([Basu and Lamprecht, 2018](#)). This model predicts a mechanism that includes a reduction in cytoskeleton dynamics and the formation of a stable blueprint of cytoskeleton structure to preserve spine morphology and memory. Our results suggest that at least a subset of cytoskeletal genes undergo increased, rather than decreased, dynamics during consolidation, which is consistent with other reports indicative of cytoskeletal dynamics in remote memory ([Jones et al., 2019](#); [Kim et al., 2014](#)). However, the changes that we found were related to the function of MT-mediated functioning of the primary cilium, rather than AF-mediated dynamics of dendritic spines, which might have retained their stability after the formation of recent memories.

The finding that the highest number of these genes was associated with primary cilium ([Figure 1B](#)) indicated that the predominant difference in cytoskeleton-mediated mechanisms during memory consolidation involves functional and/or structural changes of the primary cilium. The expression of these genes was overall increased in remote memory, suggesting a more prominent role of the primary cilium in remote memory compared to recent. Indeed, we show here that disruption of the primary cilium did not have an effect on recent memory, while it resulted in a strong impairment of remote memory ([Figures 2B](#) and [2E](#)). The role of the primary cilium in recent fear conditioning memory has been evaluated previously ([Amador-Arjona et al., 2011](#); [Berbari et al., 2014](#); [Rhee et al., 2016](#); [Wang et al., 2011](#)), and these findings were either consistent with ours, and showed no impairment of recent fear conditioning memory when the primary cilium was inhibited ([Amador-Arjona et al., 2011](#); [Wang et al., 2011](#)), or showed a small impairment, when a very large number of animals were used ([Berbari et al., 2014](#); [Rhee et al., 2016](#)). Overall, these and our data suggest that the primary cilium is not critical for recent memory, or is minimally involved at best, but it plays a substantial role in remote memory. Acute inhibition of the main cilium signaling pathway in the adult brain, Shh ([Bezard et al., 2003](#); [Breunig et al., 2008](#); [Louvi and Grove, 2011](#); [Petrova and Joyner, 2014](#); [Yao et al., 2016](#)), did not affect memory retrieval ([Figure 2F](#)), suggesting that the primary cilium contributes to consolidation rather than retrieval mechanisms. We cannot, however, completely exclude a contribution of the primary cilium to retrieval mediated by other signaling pathways ([Wheway et al., 2018](#)).

Although the exact mechanisms through which non-synaptic signaling involving the primary cilium regulates memory consolidation remain to be discovered, regulation of PNN integrity is a likely mechanism. PNNs, whose dynamic regulation is vital for consolidation ([Banerjee et al., 2017](#)), consist of ECM proteins that are very long-lived ([Toyama and Hetzer, 2013](#)), providing a stable structure that serves as a template for

long-term memory storage (Tsien, 2013). The primary cilium has access to a different extracellular environment, especially to various components of ECM, which also undergo extensive reorganization during remote memory (Nguyen et al., 2020; Tsien, 2013). The primary cilium is an important regulator of ECM composition and dynamics, either by mediating ECM protein trafficking and secretion (Noda et al., 2016; Smits et al., 2010), or through the transcriptional control of the expression of ECM-degrading proteases (Chang et al., 2012; Rockel et al., 2016). Importantly, our results suggest that consolidation of memory involves the collagen component of PNNs, rather than CSPGs. Selective manipulations targeting individual collagen genes will further elucidate their roles in stabilization of memory and PNN.

It is possible that the primary cilium also mediates consolidation through mechanisms other than the regulation of ECM. An alternative or additional mechanism is the regulation of transcriptional activity. The primary cilium forms a direct signaling connection with the nucleus, serving as a dynamic storage compartment for nuclear signaling molecules, which leave the primary cilium upon specific stimulation and translocate to the nucleus to reprogram gene expression (Satir and Satir, 2019). This direct effect on the transcriptional program could override distant synaptic signaling, particularly as the function of the primary cilium increases over time.

It is important to note that the cytoskeleton-signaling pathway is one of the top canonical pathways among differentially expressed genes in patients with stress-related disorders (Kuan et al., 2017; Mehta et al., 2017). These disorders are etiologically linked to the dysregulation of memory (van Marle, 2015), although they often develop a long time after encoding. Our experiments with the gaboxadol model of state-dependent memory identify cilium genes as potential contributors to stress pathologies, such as traumatic amnesia, as discussed in depth recently (Radulovic et al., 2018). Such memories, characterized by restricted access to retrieval and impaired consolidation, could result, at least in some cases, from impairment of the primary cilium function. Coincidentally, animal models of stress-related disorders show alterations of ECM in the CA1 region following stress, but not in other subfields of the hippocampus (Koskinen et al., 2020; Riga et al., 2017). These alterations of ECM contribute to stress-induced memory impairments, which can be reversed with the manipulations of ECM (Riga et al., 2017).

Together, our results provide an insight into general cytoskeleton-mediated mechanisms of consolidation and retrieval of aversive memories, as well as mechanisms characterized by impaired long-term consolidation. Further in-depth analyses of individual cytoskeleton-associated genes will provide novel therapeutic targets for treatments that would facilitate the retrieval of aversive memories with restricted access, and aid in the treatment of memory abnormalities occurring in psychiatric, and possibly neurological disorders. Proteins encoded by these genes are particularly attractive therapeutic targets since many drugs targeting these proteins are already approved for the treatment of other disorders, and could be repurposed, which would be a time- and cost-effective method to introduce novel treatments (Pushpakom et al., 2018).

Limitations of study

Our results have few limitations that would require additional studies to fully resolve. (1) We show here that a large number of primary cilium-associated genes are upregulated during transition of memories from recent to remote. However, our studies do not identify the mechanism and transcriptional factors involved in the activation of these genes. (2) To show that the primary cilium is not involved in memory retrieval, we blocked Shh signaling prior to recent and remote memory tests. However, although Shh is the signaling pathway most strongly linked to the primary cilium (Louvi and Grove, 2011), and strongly involved in numerous neuronal functions (Bezard et al., 2003; Breunig et al., 2008; Petrova and Joyner, 2014; Yao et al., 2016), additional experiments could exclude the involvement of one of the less prominent primary cilium signaling pathways (Whewey et al., 2018). (3) Our data show that primary cilium-mediated mechanisms, involving PNN and extracellular matrix reorganization, provide a substrate for sustained hippocampal activity, which is necessary to guide the maturation required for systems consolidation. It remains to be shown how the delayed primary cilium activity of CA1 neurons affects DH-cortical synapses involved in systems consolidation.

STAR★METHODS

Detailed methods are provided in the online version of this paper and include the following:

- KEY RESOURCES TABLE
- RESOURCE AVAILABILITY

- Lead contact
- Materials availability
- Data and code availability
- **EXPERIMENTAL MODEL AND SUBJECT DETAILS**
 - Animals
 - Primary cultures
- **METHOD DETAILS**
 - Surgery and cannulation
 - Viruses and infusions
 - Pharmacological treatments
 - Fear conditioning
 - Tissue collection
 - Proteomic analysis
 - Quantitative PCR analysis
 - RNA sequencing analysis
 - Immunohistochemistry
 - Treatments of hippocampal cultures
 - Immunofluorescence microscopy
 - Gene Ontology (GO) analysis
- **QUANTIFICATION AND STATISTICAL ANALYSIS**

SUPPLEMENTAL INFORMATION

Supplemental information can be found online at <https://doi.org/10.1016/j.isci.2021.102617>.

ACKNOWLEDGMENT

We thank Dr. Paul DeCaen (Northwestern University) for providing Arl13B-GFP P1 mice for our *in vitro* studies, and Mr. Daniel Abdella for editing the manuscript and for assistance with the manuscript preparation. This work was funded by NIMH grant MH078064 to J.R.

AUTHOR CONTRIBUTIONS

V.J. and J.R. designed the experiments, analyzed the data and wrote the manuscript. V.J. performed the experiments. H.Z. performed histological analyses of perineuronal nets. A.L.G. helped with the biochemical experiments. F.S. and A.F. performed RNA sequencing. K.V.S. and J. E. W. performed proteomic analysis.

DECLARATION OF INTERESTS

The authors declare no competing interests.

Received: December 8, 2020

Revised: April 2, 2021

Accepted: May 19, 2021

Published: June 25, 2021

REFERENCES

- Abel, T., Nguyen, P.V., Barad, M., Deuel, T.A., Kandel, E.R., and Bourchouladze, R. (1997). Genetic demonstration of a role for PKA in the late phase of LTP and in hippocampus-based long-term memory. *Cell* 88, 615–626.
- Amador-Arjona, A., Elliott, J., Miller, A., Ginbey, A., Pazour, G.J., Enikolopov, G., Roberts, A.J., and Tersikh, A.V. (2011). Primary cilia regulate proliferation of amplifying progenitors in adult Hippocampus: implications for learning and memory. *J. Neurosci.* 31, 9933.
- Banerjee, S.B., Gutzeit, V.A., Baman, J., Aoued, H.S., Doshi, N.K., Liu, R.C., and Ressler, K.J. (2017). Perineuronal nets in the adult sensory cortex are necessary for fear learning. *Neuron* 95, 169–179.e163.
- Barnes, P., Kirtley, A., and Thomas, K.L. (2012). Quantitatively and qualitatively different cellular processes are engaged in CA1 during the consolidation and reconsolidation of contextual fear memory. *Hippocampus* 22, 149–171.
- Basu, S., and Lamprecht, R. (2018). The role of actin cytoskeleton in dendritic spines in the maintenance of long-term memory. *Front. Mol. Neurosci.* 11, 143.
- Berbari, N.F., Malarkey, E.B., Yazdi, S.M., McNair, A.D., Kippe, J.M., Croyle, M.J., Kraft, T.W., and Yoder, B.K. (2014). Hippocampal and cortical primary cilia are required for aversive memory in mice. *PLoS One* 9, e106576.
- Bezard, E., Baufreton, J., Owens, G., Crossman, A.R., Dudek, H., Taupignon, A., and Brotchie, J.M. (2003). Sonic hedgehog is a neuromodulator in the adult subthalamic nucleus. *FASEB J.* 17, 2337–2338.
- Bi, A.L., Wang, Y., Li, B.Q., Wang, Q.Q., Ma, L., Yu, H., Zhao, L., and Chen, Z.Y. (2010). Region-specific involvement of actin rearrangement-

related synaptic structure alterations in conditioned taste aversion memory. *Learn. Mem. (Cold Spring Harbor, NY)* 17, 420–427.

Breunig, J.J., Sarkisian, M.R., Arellano, J.I., Morozov, Y.M., Ayoub, A.E., Sojitra, S., Wang, B., Flavell, R.A., Rakic, P., and Town, T. (2008). Primary cilia regulate hippocampal neurogenesis by mediating sonic hedgehog signaling. *Proc. Natl. Acad. Sci. U S A* 105, 13127.

Chang, C.F., Ramaswamy, G., and Serra, R. (2012). Depletion of primary cilia in articular chondrocytes results in reduced Gli3 repressor to activator ratio, increased Hedgehog signaling, and symptoms of early osteoarthritis. *Osteoarthritis Cartilage* 20, 152–161.

Cho, J., Yu, N.K., Choi, J.H., Sim, S.E., Kang, S.J., Kwak, C., Lee, S.W., Kim, J.I., Choi, D.I., Kim, V.N., et al. (2015). Multiple repressive mechanisms in the hippocampus during memory formation. *Science* 350, 82–87.

Choi, H., Tostes, R.C., and Webb, R.C. (2011). S-nitrosylation Inhibits protein kinase C-mediated contraction in mouse aorta. *J. Cardiovasc. Pharmacol.* 57, 65–71.

Coultrap, S.J., and Bayer, K.U. (2014). Nitric oxide induces Ca²⁺-independent activity of the Ca²⁺/calmodulin-dependent protein kinase II (CaMKII). *J. Biol. Chem.* 289, 19458–19465.

Daumas, S., Halley, H., Francés, B., and Lassalle, J.M. (2005). Encoding, consolidation, and retrieval of contextual memory: differential involvement of dorsal CA3 and CA1 hippocampal subregions. *Learn. Mem. (Cold Spring Harbor, NY)* 12, 375–382.

Dhiman, M., Zago, M.P., Nunez, S., Amoroso, A., Rementeria, H., Doussset, P., Nunez Burgos, F., and Garg, N.J. (2012). Cardiac-oxidized antigens are targets of immune recognition by antibodies and potential molecular determinants in chagas disease pathogenesis. *PLoS One* 7, e28449.

Dityatev, A., and Rusakov, D.A. (2011). Molecular signals of plasticity at the tetrapartite synapse. *Curr. Opin. Neurobiol.* 21, 353–359.

Fanara, P., Husted, K.H., Selle, K., Wong, P.Y., Banerjee, J., Brandt, R., and Hellerstein, M.K. (2010). Changes in microtubule turnover accompany synaptic plasticity and memory formation in response to contextual fear conditioning in mice. *Neuroscience* 168, 167–178.

Fawcett, J.W., Oohashi, T., and Pizzorusso, T. (2019). The roles of perineuronal nets and the perinodal extracellular matrix in neuronal function. *Nat. Rev. Neurosci.* 20, 451–465.

Federighi, G., Traina, G., Macchi, M., Ciampini, C., Bernardi, R., Baldi, E., Bucherelli, C., Brunelli, M., and Scuri, R. (2013). Modulation of gene expression in contextual fear conditioning in the rat. *PLoS One* 8, e80037.

Fischer, A., Sananbenesi, F., Schrick, C., Spiess, J., and Radulovic, J. (2004). Distinct roles of hippocampal de novo protein synthesis and actin rearrangement in extinction of contextual fear. *J. Neurosci.* 24, 1962–1966.

Frankland, P.W., and Bontempi, B. (2005). The organization of recent and remote memories. *Nat. Rev. Neurosci.* 6, 119–130.

Franklin, K.B.J., and Paxinos, G. (2013). *Paxinos and Franklin's the Mouse Brain in Stereotaxic Coordinates* (Academic Press).

Gao, C., Gill, M.B., Tronson, N.C., Guede, A.L., Guzman, Y.F., Huh, K.H., Corcoran, K.A., Swanson, G.T., and Radulovic, J. (2010). Hippocampal NMDA receptor subunits differentially regulate fear memory formation and neuronal signal propagation. *Hippocampus* 20, 1072–1082.

Halder, R., Hennion, M., Vidal, R.O., Shomroni, O., Rahman, R.U., Rajput, A., Centeno, T.P., van Bebber, F., Capece, V., Vizcaino, J.C.G., et al. (2016a). DNA methylation changes in plasticity genes accompany the formation and maintenance of memory. *Nat. Neurosci.* 19, 102–110.

Halder, R., Hennion, M., Vidal, R.O., Shomroni, O., Rahman, R.U., Rajput, A., Centeno, T.P., van Bebber, F., Capece, V., Garcia Vizcaino, J.C., et al. (2016b). DNA methylation changes in plasticity genes accompany the formation and maintenance of memory. *Nat. Neurosci.* 19, 102–110.

Haycraft, C.J., Zhang, Q., Song, B., Jackson, W.S., Detloff, P.J., Serra, R., and Yoder, B.K. (2007). Intraflagellar transport is essential for endochondral bone formation. *Development* 134, 307–316.

Hou, Y.Y., Lu, B., Li, M., Liu, Y., Chen, J., Chi, Z.Q., and Liu, J.G. (2009). Involvement of actin rearrangements within the amygdala and the dorsal hippocampus in aversive memories of drug withdrawal in acute morphine-dependent rats. *J. Neurosci.* 29, 12244–12254.

Hylin, M.J., Orsi, S.A., Moore, A.N., and Dash, P.K. (2013). Disruption of the perineuronal net in the hippocampus or medial prefrontal cortex impairs fear conditioning. *Learn. Mem. (Cold Spring Harbor, NY)* 20, 267–273.

Impey, S., Smith, D.M., Obrietan, K., Donahue, R., Wade, C., and Storm, D.R. (1998). Stimulation of cAMP response element (CRE)-mediated transcription during contextual learning. *Nat. Neurosci.* 1, 595–601.

Jaworski, J., Kapitein, L.C., Gouveia, S.M., Dordland, B.R., Wulf, P.S., Grigoriev, I., Camera, P., Spangler, S.A., Di Stefano, P., Demmers, J., et al. (2009). Dynamic microtubules regulate dendritic spine morphology and synaptic plasticity. *Neuron* 61, 85–100.

Ji, J., and Maren, S. (2008). Differential roles for hippocampal areas CA1 and CA3 in the contextual encoding and retrieval of extinguished fear. *Learn. Mem. (Cold Spring Harbor, NY)* 15, 244–251.

Jones, M.E., Sillivan, S.E., Jamieson, S., Rumbaugh, G., and Miller, C.A. (2019). microRNA mir-598-3p mediates susceptibility to stress enhancement of remote fear memory. *Learn. Mem. (Cold Spring Harbor, NY)* 26, 363–372.

Jovasevic, V., Corcoran, K.A., Leaderbrand, K., Yamawaki, N., Guede, A.L., Chen, H.J., Shepherd, G.M., and Radulovic, J. (2015). GABAergic mechanisms regulated by miR-33 encode state-dependent fear. *Nat. Neurosci.* 18, 1265–1271.

Kelwick, R., Desanlis, I., Wheeler, G.N., and Edwards, D.R. (2015). The ADAMTS (A disintegrin and metalloproteinase with thrombospondin motifs) family. *Genome Biol.* 16, 113.

Kim, I.H., Wang, H., Soderling, S.H., and Yasuda, R. (2014). Loss of Cdc42 leads to defects in synaptic plasticity and remote memory recall. *eLife* 3, e02839.

Koskinen, M.K., van Mourik, Y., Smit, A.B., Riga, D., and Spijker, S. (2020). From stress to depression: development of extracellular matrix-dependent cognitive impairment following social stress. *Sci. Rep.* 10, 17308.

Kuan, P.F., Waszczuk, M.A., Kotov, R., Clouston, S., Yang, X., Singh, P.K., Glenn, S.T., Cortes Gomez, E., Wang, J., Bromet, E., et al. (2017). Gene expression associated with PTSD in World Trade Center responders: an RNA sequencing study. *Transl Psychiatry* 7, 1297.

Kypri, E., Christodoulou, A., Maimaris, G., Lethan, M., Markaki, M., Lysandrou, C., Lederer, C.W., Tavernarakis, N., Geimer, S., Pedersen, L.B., et al. (2014). The nucleotide-binding proteins Nupb1 and Nupb2 are negative regulators of ciliogenesis. *Cell Mol. Life Sci.* 71, 517–538.

Lee, I., and Kesner, R.P. (2004). Differential contributions of dorsal hippocampal subregions to memory acquisition and retrieval in contextual fear-conditioning. *Hippocampus* 14, 301–310.

Levenson, J.M., Choi, S., Lee, S.Y., Cao, Y.A., Ahn, H.J., Worley, K.C., Pizzi, M., Liou, H.C., and Sweatt, J.D. (2004). A bioinformatics analysis of memory consolidation reveals involvement of the transcription factor c-rel. *J. Neurosci.* 24, 3933–3943.

Levy, A.D., Omar, M.H., and Koleske, A.J. (2014). Extracellular matrix control of dendritic spine and synapse structure and plasticity in adulthood. *Front. Neuroanat.* 8, 116.

Li, H., Handsaker, B., Wysoker, A., Fennell, T., Ruan, J., Homer, N., Marth, G., Abecasis, G., and Durbin, R. (2009). The sequence alignment/map format and SAMtools. *Bioinformatics* 25, 2078–2079.

Lienhard, M., Grimm, C., Morkel, M., Herwig, R., and Chavez, L. (2014). MEDIPS: genome-wide differential coverage analysis of sequencing data derived from DNA enrichment experiments. *Bioinformatics (Oxford, England)* 30, 284–286.

Louvi, A., and Grove, E.A. (2011). Cilia in the CNS: the quiet organelle claims center stage. *Neuron* 69, 1046–1060.

Malicki, J.J., and Johnson, C.A. (2017). The cilium: cellular antenna and central processing unit. *Trends Cell Biol.* 27, 126–140.

Matus, A. (2000). Actin-based plasticity in dendritic spines. *Science* 290, 754–758.

Mehta, D., Bruenig, D., Carrillo-Roa, T., Lawford, B., Harvey, W., Morris, C.P., Smith, A.K., Binder, E.B., Young, R.M., and Voisey, J. (2017). Genomewide DNA methylation analysis in combat veterans reveals a novel locus for PTSD. *Acta Psychiatr. Scand.* 136, 493–505.

Mei, B., Li, C., Dong, S., Jiang, C.H., Wang, H., and Hu, Y. (2005). Distinct gene expression

- profiles in hippocampus and amygdala after fear conditioning. *Brain Res. Bull.* 67, 1–12.
- Meyer, M.A.A., Corcoran, K.A., Chen, H.J., Gallego, S., Li, G., Tiruveedhula, V.V., Cook, J.M., and Radulovic, J. (2017). Neurobiological correlates of state-dependent context fear. *Learn. Mem.* (Cold Spring Harbor, NY) 24, 385–391.
- Mizuno, K., Jeffries, A.R., Abel, T., and Giese, K.P. (2020). Long-lasting transcription in hippocampal area CA1 after contextual fear conditioning. *Neurobiol. Learn. Mem.* 172, 107250.
- Murakami, T., Murakami, T., Su, W.D., Ohtsuka, A., Abe, K., and Ninomiya, Y. (1999). Perineuronal nets of proteoglycans in the adult mouse brain are digested by collagenase. *Arch. Histol. Cytol.* 62, 199–204.
- Nelson, B.S., Witty, C.F., Williamson, E.A., and Daniel, J.M. (2012). A role for hippocampal actin rearrangement in object placement memory in female rats. *Neurobiol. Learn. Mem.* 98, 284–290.
- Nestler, E.J., and Greengard, P. (1999). Protein phosphorylation is of fundamental importance in biological regulation. In *Basic Neurochemistry: Molecular, Cellular and Medical Aspects*, G.J. Siegel, B.W. Agranoff, R.W. Albers, S.K. Fisher, and M.D. Uhler, eds. (Lippincott-Raven).
- Nguyen, P.T., Dorman, L.C., Pan, S., Vainchtein, I.D., Han, R.T., Nakao-Inoue, H., Taloma, S.E., Barron, J.J., Molofsky, A.B., Kheirbek, M.A., et al. (2020). Microglial remodeling of the extracellular matrix promotes synapse plasticity. *Cell* 182, 388–403.e315.
- Noda, K., Kitami, M., Kitami, K., Kaku, M., and Komatsu, Y. (2016). Canonical and noncanonical intraflagellar transport regulates craniofacial skeletal development. *Proc. Natl. Acad. Sci. U S A* 113, E2589–E2597.
- Novak, U., and Kaye, A.H. (2000). Extracellular matrix and the brain: components and function. *J. Clin. Neurosci.* 7, 280–290.
- Parato, J., Shen, H., and Smith, S.S. (2019). alpha4betadelta GABAA receptors trigger synaptic pruning and reduce dendritic length of female mouse CA3 hippocampal pyramidal cells at puberty. *Neuroscience* 398, 23–36.
- Peixoto, L.L., Wimmer, M.E., Poplawski, S.G., Tudor, J.C., Kenworthy, C.A., Liu, S., Mizuno, K., Garcia, B.A., Zhang, N.R., Giese, K., et al. (2015). Memory acquisition and retrieval impact different epigenetic processes that regulate gene expression. *BMC Genomics* 16 (Suppl 5), S5.
- Petrova, R., and Joyner, A.L. (2014). Roles for Hedgehog signaling in adult organ homeostasis and repair. *Development* (Cambridge, England) 141, 3445–3457.
- Poplawski, S.G., Peixoto, L., Porcari, G.S., Wimmer, M.E., McNally, A.G., Mizuno, K., Giese, K.P., Chatterjee, S., Koberstein, J.N., Risso, D., et al. (2016). Contextual fear conditioning induces differential alternative splicing. *Neurobiol. Learn. Mem.* 134 (Pt B), 221–235.
- Poulos, A.M., Mehta, N., Lu, B., Amir, D., Livingston, B., Santarelli, A., Zhuravka, I., and Fanselow, M.S. (2016). Conditioning- and time-dependent increases in context fear and generalization. *Learn. Mem.* (Cold Spring Harbor, NY) 23, 379–385.
- Pushpakom, S., Iorio, F., Eyers, P.A., Escott, K.J., Hopper, S., Wells, A., Doig, A., Williams, T., Latimer, J., McNamee, C., et al. (2018). Drug repurposing: progress, challenges and recommendations. *Nat. Rev. Drug Discov.* 18, 41–58.
- Radulovic, J., Lee, R., and Ortony, A. (2018). State-dependent memory: neurobiological advances and prospects for translation to dissociative amnesia. *Front. Behav. Neurosci.* 12, 259.
- Radulovic, J., Ruhmann, A., Liepold, T., and Spiess, J. (1999). Modulation of learning and anxiety by corticotropin-releasing factor (CRF) and stress: differential roles of CRF receptors 1 and 2. *J. Neurosci.* 19, 5016–5025.
- Radulovic, J., and Tronson, N.C. (2010). Molecular specificity of multiple hippocampal processes governing fear extinction. *Rev. Neurosci.* 21, 1–17.
- Rao-Ruiz, P., Couey, J.J., Marcelo, I.M., Bouwkamp, C.G., Slump, D.E., Matos, M.R., van der Loo, R.J., Martins, G.J., van den Hout, M., van I.W.F., et al. (2019). Engram-specific transcriptome profiling of contextual memory consolidation. *Nat. Commun.* 10, 2232.
- Reichelt, A.C., Hare, D.J., Bussey, T.J., and Saksida, L.M. (2019). Perineuronal nets: plasticity, protection, and therapeutic potential. *Trends Neurosci.* 42, 458–470.
- Remondes, M., and Schuman, E.M. (2004). Role for a cortical input to hippocampal area CA1 in the consolidation of a long-term memory. *Nature* 431, 699–703.
- Revest, J.M., Kaoouane, N., Mondin, M., Le Roux, A., Rouge-Pont, F., Vallee, M., Barik, J., Tronche, F., Desmedt, A., and Piazza, P.V. (2010). The enhancement of stress-related memory by glucocorticoids depends on synapsin-1a/lb. *Mol. Psychiatry* 15, 1140–1151, 1125.
- Rhee, S., Kirschen, G.W., Gu, Y., and Ge, S. (2016). Depletion of primary cilia from mature dentate granule cells impairs hippocampus-dependent contextual memory. *Sci. Rep.* 6, 34370.
- Riga, D., Kramvis, I., Koskinen, M.K., van Bokhoven, P., van der Harst, J.E., Heistek, T.S., Jaap Timmerman, A., van Nierop, P., van der Schors, R.C., Pieneman, A.W., et al. (2017). Hippocampal extracellular matrix alterations contribute to cognitive impairment associated with a chronic depressive-like state in rats. *Sci. Transl. Med.* 9, eaai8753.
- Rockel, J.S., Yu, C., Whetstone, H., Craft, A.M., Reilly, K., Ma, H., Tsumaha, H., Puvindran, V., Al-Jazrawe, M., Keller, G.M., et al. (2016). Hedgehog inhibits β -catenin activity in synovial joint development and osteoarthritis. *J. Clin. Invest.* 126, 1649–1663.
- Romberg, C., Yang, S., Melani, R., Andrews, M.R., Horner, A.E., Spillantini, M.G., Bussey, T.J., Fawcett, J.W., Pizzorusso, T., and Saksida, L.M. (2013). Depletion of perineuronal nets enhances recognition memory and long-term depression in the perirhinal cortex. *J. Neurosci.* 33, 7057–7065.
- Satir, P., and Satir, B.H. (2019). The conserved ancestral signaling pathway from cilium to nucleus. *J. Cell Sci.* 132.
- Schlessinger, J. (2000). Cell signaling by receptor tyrosine kinases. *Cell* 103, 211–225.
- Sethi, M.K., and Zaia, J. (2017). Extracellular matrix proteomics in schizophrenia and Alzheimer's disease. *Anal. Bioanal. Chem.* 409, 379–394.
- Shumyatsky, G.P., Malleret, G., Shin, R.M., Takizawa, S., Tully, K., Tsvetkov, E., Zakharenko, S.S., Joseph, J., Vronskaia, S., Yin, D., et al. (2005). stathmin, a gene enriched in the amygdala, controls both learned and innate fear. *Cell* 123, 697–709.
- Sullivan, S.E., Joseph, N.F., Jamieson, S., King, M.L., Chevere-Torres, I., Fuentes, I., Shumyatsky, G.P., Brantley, A.F., Rumbaugh, G., and Miller, C.A. (2017). Susceptibility and resilience to posttraumatic stress disorder-like behaviors in inbred mice. *Biol. Psychiatry* 82, 924–933.
- Smits, P., Bolton, A.D., Funari, V., Hong, M., Boyden, E.D., Lu, L., Manning, D.K., Dwyer, N.D., Moran, J.L., Prysak, M., et al. (2010). Lethal skeletal dysplasia in mice and humans lacking the golgin GMAP-210. *N. Engl. J. Med.* 362, 206–216.
- Su, J., Cole, J., and Fox, M.A. (2017). Loss of interneuron-derived collagen XIX leads to a reduction in perineuronal nets in the mammalian telencephalon. *ASN Neuro* 9, 1759091416689020.
- Szklarczyk, D., Gable, A.L., Lyon, D., Junge, A., Wyder, S., Huerta-Cepas, J., Simonovic, M., Doncheva, N.T., Morris, J.H., Bork, P., et al. (2019). STRING v11: protein-protein association networks with increased coverage, supporting functional discovery in genome-wide experimental datasets. *Nucleic Acids Res.* 47, D607–D613.
- Tada, T., and Sheng, M. (2006). Molecular mechanisms of dendritic spine morphogenesis. *Curr. Opin. Neurobiol.* 16, 95–101.
- Thompson, E.H., Lensjø, K.K., Wigestrand, M.B., Malthe-Sørensen, A., Hafting, T., and Fyhn, M. (2018). Removal of perineuronal nets disrupts recall of a remote fear memory. *Proc. Natl. Acad. Sci. U S A* 115, 607–612.
- Tonegawa, S., Morrissey, M.D., and Kitamura, T. (2018). The role of engram cells in the systems consolidation of memory. *Nat. Rev. Neurosci.* 19, 485–498.
- Toyama, B.H., and Hetzer, M.W. (2013). Protein homeostasis: live long, won't prosper. *Nat. Rev. Mol. Cell Biol.* 14, 55–61.
- Tsien, R.Y. (2013). Very long-term memories may be stored in the pattern of holes in the perineuronal net. *Proc. Natl. Acad. Sci. U S A* 110, 12456–12461.
- Uchida, S., Martel, G., Pavlovsky, A., Takizawa, S., Hevi, C., Watanabe, Y., Kandel, E.R., Alarcon, J.M., and Shumyatsky, G.P. (2014). Learning-induced and stathmin-dependent changes in microtubule stability are critical for memory and disrupted in ageing. *Nat. Commun.* 5, 4389.
- Uddin, B., Partscht, P., Chen, N.P., Neuner, A., Weiss, M., Hardt, R., Jafarpour, A., Hessler, B.,

Ruppert, T., Lorenz, H., et al. (2019). The human phosphatase CDC14A modulates primary cilium length by regulating centrosomal actin nucleation. *EMBO Rep.* 20, e46544.

van Marle, H. (2015). PTSD as a memory disorder. *Eur. J. Psychotraumatol.* 6. <https://doi.org/10.3402/ejpt.v3406.27633>.

Wang, Z., Phan, T., and Storm, D.R. (2011). The type 3 adenylyl cyclase is required for novel object learning and extinction of contextual memory: role of cAMP signaling in primary cilia. *J. Neurosci.* 31, 5557–5561.

Warde-Farley, D., Donaldson, S.L., Comes, O., Zuberi, K., Badrawi, R., Chao, P., Franz, M., Grouios, C., Kazi, F., Lopes, C.T., et al. (2010). The GeneMANIA prediction server: biological network integration for gene prioritization and predicting gene function. *Nucleic Acids Res.* 38, W214–W220.

Wen, J.J., Zago, M.P., Nunez, S., Gupta, S., Burgos, F.N., and Garg, N.J. (2012). Serum proteomic signature of novel potential protein biomarkers of disease. *Mol. Cell. Proteomics* 11, 435–452.

Wheway, G., Nazlamova, L., and Hancock, J.T. (2018). Signaling through the primary cilium. *Front. Cell Dev. Biol.* 6, 8.

Wiktorowicz, J.E., Chowdhury, I.H., Stafford, S., Choudhuri, S., Dey, N., and Garg, N.J. (2019). Integrated functional analysis of the nuclear proteome of classically and alternatively activated macrophages. *Mediators Inflamm.* 2019, 19.

Wiktorowicz, J.E., Stafford, S.J., and Garg, N.J. (2017). Protein cysteinyl-S-nitrosylation: analysis and quantification. *Methods Enzymol.* 586, 1–14.

Wingett, S.W., and Andrews, S. (2018). FastQ Screen: a tool for multi-genome mapping and quality control. *F1000Res.* 7, 1338.

Yao, P.J., Petralia, R.S., and Mattson, M.P. (2016). Sonic hedgehog signaling and hippocampal neuroplasticity. *Trends Neurosci.* 39, 840–850.

Yasukawa, T., Tokunaga, E., Ota, H., Sugita, H., Martyn, J.A., and Kaneki, M. (2005). S-nitrosylation-dependent inactivation of Akt/protein kinase B in insulin resistance. *J. Biol. Chem.* 280, 7511–7518.

Zago, M.P., Wiktorowicz, J.E., Spratt, H., Koo, S.J., Barrientos, N., Nunez Burgos, A., Nunez Burgos, J., Iniguez, F., Botelli, V., Leon de la Fuente, R., et al. (2018). Potential utility of protein targets of cysteine-S-nitrosylation in identifying clinical disease status in human chagas disease. *Front. Microbiol.* 9, 3320.

STAR★METHODS

KEY RESOURCES TABLE

REAGENT or RESOURCE	SOURCE	IDENTIFIER
Antibodies		
adenylate cyclase 3	EnCor Biotechnology	Cat#: MCA-1A12; RRID:AB_2744501
Alexa Fluor 594 AffiniPure Donkey Anti-Mouse IgG (H+L)	Jackson ImmunoResearch	Cat#: 715-585-150; RRID:AB_2340854
GFP-Booster Alexa Fluor 488	Chromotek	Cat#: gb2AF488-10; RRID:AB_2827573
Bacterial and virus strains		
AAV-DJ/8-U6-GFP-m-IFT88-shRNA	Vector Biolabs	N/A
AAV/DJ8-GFP-U6-scrmb-shRNA	Vector Biolabs	N/A
Biological samples		
DH total RNA; C57BL/6N mice, naive	This paper	N/A
DH total RNA; C57BL/6N mice, 4 days post contextual fear conditioning	This paper	N/A
DH total RNA; C57BL/6N mice, 21 days post contextual fear conditioning	This paper	N/A
Coronal brain sections; C57BL/6N mice, 6 weeks after AAV/DJ8-GFP-U6-scrmb-shRNA infusion into DH	This paper	N/A
Coronal brain sections; C57BL/6N mice, 6 weeks after AAV-DJ/8-U6-GFP-m-IFT88-shRNA infusion into DH	This paper	N/A
Coronal brain sections; C57BL/6N mice, 5 days after chondroitinase ABC infusion into DH + 4 days after contextual fear conditioning	This paper	N/A
Coronal brain sections; C57BL/6N mice, 5 days after chondroitinase ABC infusion into DH + 21 days after contextual fear conditioning	This paper	N/A
DH total RNA; C57BL/6N mice, gaboxadol infusion into DH, 4 days post contextual fear conditioning	This paper	N/A
DH total RNA; C57BL/6N mice, gaboxadol infusion into DH, 21 days post contextual fear conditioning	This paper	N/A
DH total protein; C57BL/6N mice, ACSF infusion into DH, 24 h post contextual fear conditioning	This paper	N/A
DH total protein; C57BL/6N mice, gaboxadol infusion into DH, 24 h post contextual fear conditioning	This paper	N/A
Coronal brain sections; Grin2a ^{tm1NaK} mice	This paper	N/A
Arl13B-GFP hippocampal neurons, DIV 14, vehicle + vehicle treated; paraformaldehyde fixed	This paper	N/A
Arl13B-GFP hippocampal neurons, DIV 14, gaboxadol + vehicle treated; paraformaldehyde fixed;	This paper	N/A

(Continued on next page)

Continued

REAGENT or RESOURCE	SOURCE	IDENTIFIER
Arl13B-GFP hippocampal neurons, DIV 14, vehicle + NMDA treated; paraformaldehyde fixed	This paper	N/A
Arl13B-GFP hippocampal neurons, 14 DIV, gaboxadol + NMDA treated; paraformaldehyde fixed	This paper	N/A
C57BL/6N hippocampal neurons, DIV 14, AAV/DJ8-GFP-U6-scrmb-shRNAtansduced; paraformaldehyde fixed	This paper	N/A
C57BL/6N hippocampal neurons, DIV 14, AAV-DJ/8-U6-GFP-m-IFT88-shRNAtansduced; paraformaldehyde fixed	This paper	N/A
Chemicals, peptides, and recombinant proteins		
Gaboxadol hydrochloride	Millipore-Sigma	Cat#: T101
Cyclopamine, V. californicum	Millipore-Sigma	Cat#: 239803
Chondroitinase ABC	Amsbio	Cat#: E1028-10
BODIPY FL N-(2-aminoethyl) maleimide	ThermoFisher	Ca#: B10250
Pro-Q Diamond Phosphoprotein Gel Stain	ThermoFisher	Cat#: P33300
2, 2, 2-tribromoethanol 99%	ThermoFisher	Cat#: AAA1870614
Biotinylated Wisteria Floribunda Lectin	Vector Biolaboratories	Cat#: B-1355-2
Carbo-Free Blocking Solution	Vector Biolaboratories	Cat#: SP-5040-125
FluorSave	Millipore-Sigma	345789-20ML
Critical commercial assays		
miRCURY RNA Isolation Kit-Tissue	Qiagen/Exiqon	Cat#: 300111
TaqMan Reverse Transcription Reagents	ThermoFisher	Cat#: N8080234
SYBR green detection system	ThermoFisher	Cat#: 4368706
TruSeq RNA Sample Preparation v2 Kit	Illumina	Cat#: RS-122-2001, RS-122-2002
Qubit dsDNA HS Assay kit	ThermoFisher	Ca#: Q32851
VECTASTAIN Elite ABC HRP Kit (Peroxidase, Standard) PK6100	ThermoFisher	Cat#: NC9313719
Experimental models: cell lines		
C57BL/6N DIV14 primary hippocampal cells; male, female	This paper	N/A
Arl13B-GFP DIV14 primary hippocampal cells; male, female	This paper	N/A
Experimental models: organisms/strains		
C57BL/6N mice	Envigo	N/A
Grin2a ^{tm1NaK} mice	Jackson Laboratory	N/A
Arl13B-GFP mice	Dr. Paul DeCaen, Northwestern University	N/A
Oligonucleotides		
Mm_Fhdc1_1_SG QuantiTect Primer Assay	Qiagen	ID#: QT01052968
Mm_Dnaaf1_1_SG QuantiTect Primer Assay	Qiagen	ID#: QT00172942
Mm_Fbxl13_1_SG QuantiTect Primer Assay	Qiagen	ID#: QT00176736
Mm_B930008I02Rik_1_SG QuantiTect Primer Assay	Qiagen	ID#: QT00136437

(Continued on next page)

Continued		
REAGENT or RESOURCE	SOURCE	IDENTIFIER
Software and algorithms		
SameSpots v4.6	TotalLab	http://totalab.com/samespots
Protein Prophet algorithm	National Institutes of Health	http://proteinprophet.sourceforge.net
FastQC v0.10.1	Babraham Institute	http://www.bioinformatics.babraham.ac.uk/projects/fastqc
SAMtools flagstat v0.1.18	The Wellcome Trust Sanger Institute	http://www.htslib.org/
MEDIPS R package section 2.4.2	Bioconductor	https://bioconductor.org/packages/release/bioc/html/MEDIPS.html
STAR aligner58 2.3.0e_r291	Cold Spring Harbor Laboratory	http://code.google.com/p/ma-star
FeaturesCount	The Walter and Eliza Hall Institute of Medical Research	bioinf.wehi.edu.au/featureCounts
Imaris	Oxford Instruments	https://imaris.oxinst.com
Prism 9	GraphPad	https://www.graphpad.com
Other		
High-Speed Amino Acid Analyzer L8800	Hitachi High Technologies	https://www.hitachi-hightech.com
IPGphor multiple-sample isoelectric focusing (IEF) device	GE Healthcare	https://www.gehealthcare.com
Criterion Dodeca cell	Bio-Rad	https://www.bio-rad.com
Typhoon Trio Variable Mode Imager	GE Healthcare	https://www.gehealthcare.com
Applied Biosystems 7500 Real-Time PCR System	ThermoFisher	https://www.thermofisher.com
2100 Bioanalyzer system	Agilent	https://www.agilent.com
Micro4-WPI microsyringe pump controller	World Precision Instruments	https://www.wpiinc.com
TSE Multi Conditioning System 256060	TSE Systems	https://www.tse-systems.com

RESOURCE AVAILABILITY

Lead contact

Further information and requests for resources and reagents should be directed to and will be fulfilled by the lead contact, Dr. Jelena Radulovic (jelena.radulovic@einsteinmed.org).

Materials availability

This study did not generate new unique reagents.

Data and code availability

The accession number for the RNA-Seq data is GEO: GSE174076. Proteomics data are available from the corresponding author on request. This study did not generate program code.

EXPERIMENTAL MODEL AND SUBJECT DETAILS

Animals

9-week-old male C57BL/6N mice were obtained from a commercial supplier (Envigo), individually housed on a 12-hr light/dark cycle (lights on at 7 AM) and allowed ad libitum access to food and water. All procedures were approved by Northwestern University's Animal Care and Use Committee in compliance with US National Institutes of Health standards. 9-week-old male N-methyl D-aspartate glutamate receptor, subunit 2A knockdown mice (*Grin2a^{tm1Nak}*) were obtained from Jackson Laboratory. One-day-old male and female pups of transgenic mice expressing ADP-ribosylation factor-like protein 13B (Arl13B) fused to GFP were obtained from Dr. Paul DeCaen (Northwestern University).

Primary cultures

The hippocampi from post-natal day 1 old (P1) Arl13B-GFP or C57BL/6N male and female mice were isolated, dissociated, and cultured as described previously (Gao et al., 2010). Briefly, cells were plated on coverslips coated with poly-d-lysine (Sigma-Aldrich) in 24-well culture plates at a density of 50,000 cells/cm² and grown in Neurobasal Medium containing 1 mM GlutaMax, and 2% B27 (all from ThermoFisher). One-half of the medium was replaced with identical medium every 4 days. Under these conditions, >85% of cells were viable, >90% of cells were neurons, and cultures could be maintained for 3 weeks. Neurons were cultured for 14 *in vitro* (DIV) before treatments.

METHOD DETAILS

Surgery and cannulation

Double-guided cannulas (Plastic One) were implanted in the dorsal hippocampus (DH) as described previously (Radulovic et al., 1999). Mice were anesthetized with 1.2% tribromoethanol (vol/vol, Avertin) and implanted with bilateral 26-gauge cannulas using a stereotaxic apparatus. Stereotaxic coordinates for the dorsal hippocampus were 1.8 mm posterior, ±1.0 mm lateral and 2.0 mm ventral to bregma, according to the mouse brain atlas (Franklin and Paxinos, 2013).

Viruses and infusions

The viral vectors carrying a construct coding for an shRNA targeting mouse IFT88 (IFT88: AAV-DJ/8-U6-GFP-m-IFT88-shRNA; Vector Biolabs), or control construct (GFP: pAAV2-CAG-GFP; Addgene) were bilaterally infused into the dorsal hippocampus (1.8 mm posterior, ±1.0 mm lateral and 2.0 mm ventral to bregma). Infusions were performed using an automatic microsyringe pump controller (Micro4-WPI) connected to a Hamilton microsyringe. The viral vectors were infused in a volume of 0.5 µL per site, at titer >8 × 10¹² GC/ml, over 2 min, and syringes were left in place for 5 min prior to removal to allow for virus diffusion.

Pharmacological treatments

Gaboxadol (0.5 µg, dissolved in artificial cerebrospinal fluid (ACSF); Millipore-Sigma), and cyclopamine (10 ng, dissolved in ACSF; Millipore-Sigma) were injected intrahippocampally (i.h.), at a volume of 0.5 µl per side, at a rate of 0.15 µl/min. Chondroitinase ABC (65 U/ml, dissolved in ACSF; Amsbio) was injected i.h., at a volume of 0.25 µl per side, at a rate of 0.15 µl/min.

Fear conditioning

Contextual fear conditioning was performed in an automated system (TSE Systems) as previously described (Radulovic et al., 1999). Briefly, mice were exposed for 3 min to a novel context, followed by a foot shock (2 s, 0.7 mA, constant current). 24 hr later, mice were tested for memory retrieval. Testing consisted of 3 min in the conditioning context, during which freezing was measured every 10 s. Freezing was expressed as a percentage of the total number of observations during which the mice were motionless. Activity was recorded automatically by an infrared beam system and expressed as cm/s. The individual experiments were not performed on littermates, so we did not apply randomization procedures, but all behavioral tests were performed by experimentalists who were unaware of the treatments. During training, blinding was performed so that a laboratory member not involved in the experiments would prepare and color code the solution. In addition, the experimenter performing the tests was not aware of the numbering code.

Tissue collection

For all analyses, mice were sacrificed by cervical dislocation, dorsal hippocampi immediately dissected and frozen in liquid nitrogen. Frozen tissue was stored at -80°C until protein or RNA extractions were performed.

Proteomic analysis

Protein extraction and identification of phosphorylated and S-nitrosylated (SNO) proteins was performed as previously described (Wiktorowicz et al., 2019): total proteins were extracted with 7 M urea, 2 M thiourea, 2% CHAPS, and 50 mM Tris pH 7.5, treated with sodium ascorbate (Asc) to reverse S-nitrosylation (SNO) and then dialyzed against the urea buffer to remove Asc. Protein concentrations were determined with

the Lowry method and cysteines (cysteic acid) determined by amino acid analysis (Model L8800, Hitachi High Technologies America, Pleasanton, CA). One aliquot of each sample (100 μ g protein) was treated with 6 mM ascorbate (Asc^+) to reduce the nitrosylated cysteine residues and make them available for dye binding, and the other aliquot (Asc^-) was treated with 100 μ M neocuproine (phenanthroline derivative and chelating agent) that blocks SNO reduction and stabilizes SNO during further processing of samples. All sample aliquots were dialyzed against urea buffer and labeled with BODIPY FL N-(2-aminoethyl) malimide (ThermoFisher) at 60-fold excess to cysteine residues for 2 h, and the reactions were stopped with 2-mercaptoethanol. The BD-labeled (Asc^+ and Asc^-) samples (100 μ g protein) were separated by 2DE, employing an IPGphor multiple-sample isoelectric focusing (IEF) device (GE Healthcare) in the first dimension, and the Criterion Dodeca cell (Bio-Rad) in the second dimension. Gels were fixed in 20% methanol/7% acetic acid/10% acetonitrile and washed with 20% ethanol/10% acetonitrile, and images for BD-labeled proteins were acquired at $\text{Ex}_{488\text{nm}}/\text{Em}_{520/40\text{nm}}$ by using a Typhoon Trio Variable Mode Imager (GE Healthcare). Since some spectral overlap can occur between BD and PQD, the gels were also scanned at $\text{Ex}_{532\text{nm}}/\text{Em}_{560\text{nm}}$ to quantify the potential BD spillover signal into the PQD window. After scanning, gels were stained for 90 min with Pro-Q Diamond (Invitrogen, Carlsbad, CA) that selectively labels the phosphoproteins in acrylamide gels, destained with 20% acetonitrile/50 mM sodium acetate (pH 4.0), and scanned with the PQD detection excitation and emission configuration to quantify the PQD fluorophore. Gel images were analyzed with SameSpots v4.6 software (TotalLab, Newcastle, U.K.). Raw spot volumes obtained from the program were used to normalize all dye set quantifications by summing the spot volume signals present within each gel and applying a bias factor to all spot volumes relative to the reference gel total spot volume. In addition, since normalization is performed to account for variable protein loading, all SNO and PQD normalizations were performed with the sample cognate Asc^+ BD gels. To obtain quantitative data on change in SNO levels, fluorescence normalized volumes of the protein spots from BD-stained Asc^- gels were calculated. The ratio-of-ratio (SNO/ Δ abundance) values were calculated to account for changes in SNO with respect to protein abundance and establish true SNO-specific changes in experimental samples with respect to controls. Moreover, it is noted that because SNO modification prevents the Cys-BODIPY labeling, a negative value indicates an increase in SNO level (and vice versa) in the sample (Wiktorowicz et al., 2017). To obtain quantitative data on change in phosphorylation levels, the BD spillover volumes for each spot were subtracted from the corresponding PQD spot value. The corrected PQD values were then normalized for protein loading differences by using the BD normalization factor of that same gel. The differential protein phosphorylation of each spot volume was then calculated.

The protein spots that exhibited significant differential phosphorylation, or SNO, were subjected to mass spectrometry identification, as previously described (Dhiman et al., 2012; Wen et al., 2012). Protein spot IDs with expectation values ≤ 0.05 were considered significant. The Protein Prophet algorithm was used to assign the protein probabilities (Zago et al., 2018).

Quantitative PCR analysis

Dorsal hippocampi were collected around the tips of the hippocampal cannulas. Total RNA was extracted using miRCURY RNA Isolation Kit-Tissue (Qiagen). Reverse transcription was performed on 100 ng of total RNA using First Strand cDNA Synthesis Kit (Applied Biosystems). Real-time PCR analysis was performed on an Applied Biosystems 7500 instrument using SYBR green detection system (ThermoFisher) and primers specific for *Fhd1*, *Dnaaf1*, *Fbxl13*, or *Ccdc40* (B930008102Rik) (all from Qiagen).

RNA sequencing analysis

Read quality was assessed using FastQC (Wingett and Andrews, 2018) (v0.10.1) to identify sequencing cycles with low average quality, adaptor contamination, or repetitive sequences from PCR amplification. Alignment quality was analyzed using SAMtools flagstat (Li et al., 2009) (v0.1.18) with default parameters. Data quality was visually inspected in a genome browser at <http://memory-epigenome-browser.dzne.de>. Furthermore, we assessed if samples were sequenced deep enough by analyzing the average per base coverage and the saturation correlation for all samples using the MEDIPS R package (Lienhard et al., 2014) (section 2.4.2). The saturation function splits each library in fractions of the initial number of reads (10 subsets of equal size) and plots the convergence. The correlation between biological replicates was evaluated using Pearson correlation (function MEDIPS.correlation). Only data passing all quality standards was used for further analyses. Data were aligned to the genome using gapped alignment as RNA transcripts are subject to splicing and reads might therefore span two distant exons. Reads were aligned to the whole *Mus musculus* mm10 genome using STAR aligner58 (2.3.0e_r291) with default options,

generating mapping files (BAM format). Reads were aligned to mouse genome *Mus musculus* mm10 and counted using FeaturesCount as described previously (Halder et al., 2016a).

Immunohistochemistry

Mice were anesthetized with an i.p. injection of 240 mg/kg Avertin and transcardially perfused with ice-cold 4% paraformaldehyde in phosphate buffer (pH 7.4, 150 ml per mouse). Brains were removed and post-fixed for 24 h in the same fixative and then immersed for 24 h each in 20 and 30% sucrose in phosphate buffer. Brains were frozen and 50 μ m sections were cut for use in free-floating immunohistochemistry (Jovasevic et al., 2015) with primary antibodies against adenylate cyclase 3 (1:1000, EnCor Biotechnology, MCA-1A12). Secondary antibodies were obtained from Jackson ImmunoResearch (1:200, Alexa Fluor® 594 AffiniPure Donkey Anti-Mouse IgG [H+L]). GFP was visualized by its intrinsic fluorescence. Sections were mounted using FluorSave (Millipore-Sigma) and observed with Nikon W1 Dual Cam Spinning Disk Confocal microscope using 100 \times objective. PNNs were visualized using Wisteria Floribunda Lectin (WFA) staining, which has been widely used as a PNN marker in histological analyses (Fawcett et al., 2019). WFA staining was performed according to manufacturer's instructions. Briefly, endogenous peroxidase was inactivated with hydrogen peroxide. Following streptavidin/biotin and Carbo-Free blocking, sections were incubated with biotinylated WFA (Vector Biolaboratories, Burlingame, CA), Vectastain ABC system, and rhodamineisothiocyanate. Sections were mounted using FluorSave (Millipore-Sigma) and observed with Leica microscope equipped with a CCD (Olympus) camera, using 10 \times objective.

Treatments of hippocampal cultures

Arl13B-GFP cells were treated with 100 μ M gaboxadol (Parato et al., 2019) for 20 min, followed by the treatment with 25 μ M NMDA for 10 min. After 24 or 48 h cells were fixed with 4% paraformaldehyde for 15 min. C57BL/6N cells were transduced with 100 \times 10⁶ GC/well of shCTRL or shIFT88 AAV vectors, and 15 days later fixed with 4% paraformaldehyde for 15 min. Live cells were examined for changes in cell morphology, as indication of cell health and viability, and for the expression of the GFP transgene constructs using a Nikon inverted microscope with CoolSNAP-EZ digital camera, on 10 \times objective.

Immunofluorescence microscopy

Primary cilia were visualized by enhancing the fluorescent GFP signal (from Arl13B-GFP) using GFP-Booster Alexa Fluor 488 antibody (Chromotek), following the manufacturer's protocol. Briefly, cells were permeabilized for 5 min with PBS containing 0.5% Triton X-100, blocked with 4% BSA in PBS for 10 min, and incubated with the GFP-Booster antibody (1:200) in blocking buffer for 1 h at room temperature. Coverslips were mounted using FluorSave reagent (MilliporeSigma). Samples were imaged on Nikon W1 spinning disc confocal microscope (Center for Advanced Microscopy, Northwestern University) using 60 \times oil objective. Z-stack was generated from 30 images with 0.5 μ m steps. Z-stacks were processed, and surface area and volume calculated using Imaris software (Oxford Instruments). The entire experiment was performed on three separately cultured sets of neurons. From each sample set 6 Z-stacks were generated, for the total of 18 stacks.

Gene Ontology (GO) analysis

Cytoskeleton-associated genes were identified by analyzing the genes identified through RNAseq in Mouse Genome Database (MGI), searching for those classified within GO term "Cytoskeletal protein" (ID: GO:0044430). This GO term is defined as any constituent part of the cytoskeleton, a cellular scaffolding or skeleton that maintains cell shape, enables some cell motion (using structures such as flagella and cilia), and plays important roles in both intra-cellular transport (e.g. the movement of vesicles and organelles) and cellular division. It includes constituent parts of intermediate filaments, microfilaments, microtubules, and the microtrabecular lattice. For the analysis of association of the cytoskeleton-associated genes with Cytoskeleton component, Cell region and Cytoskeletal transport categories, genes were analyzed in MGI Batch Query for association with Cytoskeletal part child terms to determine the number of genes within each child term. The child terms were manually classified within the three categories. To simplify presentation and interpretation of the data, the child terms that did not contain any genes in any of the experimental groups were not included in the figures, except for terms related to specific types of synapses. ECM genes were identified as those classified within GO term "Extracellular matrix" (ID: GO:0031012) in MGI. Functional protein association network analysis was performed using STRING database (version 11.0) (Szklarczyk

et al., 2019). Gene-gene functional interaction network analysis between primary cilium- and ECM-associated genes was performed using GeneMANIA prediction server (Warde-Farley et al., 2010).

QUANTIFICATION AND STATISTICAL ANALYSIS

Statistical analyses were performed using GraphPad Prism software. One-way ANOVA was followed by Tukey's test for post hoc comparisons of three or more experimental groups (only when ANOVA was significant) or Student's t test for comparison of two experimental groups. The type of statistical test that was performed for each experiment is indicated in the figure legends. Homogeneity of variance was confirmed with Levene's test for equality of variances. All comparisons were conducted using two-tailed tests and the *P* value for all cases was set to <0.05 for significant differences. *P* value ranges are indicated by asterisks (*, **, ***, ****), octothorpes (#, ##, ###, ####) and double daggers (‡, ††, †††, ††††) in figure legends. Group sizes were determined using power analysis assuming a moderate effect size of 0.5. For proteomic analyses, the spot volumes were subjected to statistical analysis by using built-in tools of TotalLab SameSpots software. The Δ phosphorylation and RoR values for all protein spots between any two groups were subjected to statistical analysis by Student's t test with Welch's correction for unequal variances. Also, to account for the false discovery rate, Benjamini-Hochberg (B-H) multiple hypothesis testing correction was applied, and significance was accepted at *p* value ≤ 0.05 . All proteins/genes with significant differences in post-translational modification/expression were used for subsequent analyses. Primary cilium size data were analyzed using two-way ANOVA with group (vehicle or gaboxadol) and post-NMDA time length as factors. When significant main and interaction effects were observed, two-way ANOVA was followed by Sidak's multiple comparison tests.